# NEB in Analysis of Natural Image $8 \times 8$ and $9 \times 9$ High-contrast Patches

Shengxiang Xia
School of Science,
Shandong Jianzhu University,
Jinan 250101 P.R.China.

Wen Wang
School of Science,
Shandong Jianzhu University,
Jinan 250101 P.R.China.

***Abstract*—In this paper we use the nudged elastic band technique from computational chemistry to investigate sampled high-dimensional data from a natural image database. We randomly sample $8\times8$ and $9\times9$ high-contrast patches of natural images and create a density estimator believed as a Morse function. By the Morse function we build one-dimensional cell complexes from the sampled data. Using one-dimensional cell complexes, we identify topological properties of $8 \times 8$ and $9 \times 9$ high-contrast natural image patches, we show that there exist two kinds of subsets of high-contrast $8 \times 8$ and $9 \times 9$ patches modeled as a circle, by the new method we confirm some results obtained through the method of computational topology.**

***Keywords*—nudged elastic band; natural image high-contrast patch; cell complex; density function**

## I. Introduction

Computational topology becomes a very important and efficiently method to analyse high-dimensional dada in the recent years [1], [2], [3], [4]. To analyse high-dimensional dada, we usually construct a sequence of simplicial complexes from the finite sampled data set to produce a simple combinatorial presentations of the data, the most commonly used complexes include Čech complexes, Rips complexes and lazy witness complexes. As the dimensional problem, the constructed simplicial complexes usually compose of thousands (even tens of thousands) of simplices , they are sometimes too large to compute. Adams, Atanasov, and Carlsson [5] used the nudged elastic band method to construct cell complexes through density functions of sampling data, they built more low-priced reasonable models for some nonlinear data sets (such as, sets generated from social networks, from range image analysis, and from microarray analysis) by a few of cell complexes, and effectively detect the homology of the nonlinear data sets, it initially shows that cell complex models are efficient ways for analysing high-dimensional nonlinear data. Adams etc [5] obtained a circle model and the three circle model for the data set of $3 \times 3$ optical image patches from [6]. In the paper [7], Xia shown that there exist some core subsets of $8 \times 8$ and $9 \times 9$ natural image patches that are topologically equivalent to a circle and the three circle model respectively.

In this paper, we utilize the methods of the paper [5] to identify topological features of spaces of $8 \times 8$ and $9 \times 9$ natural image patches, we discover a circle model for $8 \times 8$ and $9 \times 9$ patches. The data sets used here are drawn from INRIA Holidays dataset [8], that are different from the data set in the paper [5].

## II. Basic Concepts

### A. Nudged elastic band

The nudged elastic band (NEB) is an effective way for finding a minimum energy path between two initial stable states. The minimum energy path have the property of any point on the path being at an energy minimum in all directions perpendicular to the path [9].

An elastic band with $N + 1$ images can be defined by $[\mathbf{U}_0, \mathbf{U}_1, ..., \mathbf{U}_N]$, $\mathbf{U}_0$ and $\mathbf{U}_N$ are initial and final states. The $N - 1$ middle images are modified by an optimization algorithm [11].

The total force acting on each image is defined as following:

$$\begin{aligned}\mathbf{F}_i = \mathbf{F}_i^S|_{\|} - \bigtriangledown E(\mathbf{U}_i)|_{\perp} = (||\mathbf{U}_{i+1} - \mathbf{U}_i|| \\ -||\mathbf{U}_i - \mathbf{U}_{i-1}||)\tau_i - (\bigtriangledown E(\mathbf{U}_i) - \bigtriangledown E(\mathbf{U}_i) \cdot \tau_i),\end{aligned} \quad (1)$$

the first part $\mathbf{F}_i^S|_{\|}$ is called the spring force, the second part $\bigtriangledown E(\mathbf{U}_i)|_{\perp}$ is true force, and $\tau_i = \frac{(\mathbf{U}_{i+1}-\mathbf{U}_{i-1})}{||\mathbf{U}_{i+1}-\mathbf{U}_{i-1}||}$ local tangent at image $i$. where $E$ is the energy of the system.

The nudged elastic band method apply an optimization algorithm to shift the images depending to the force in (1) for finding the minimum energy path. For more details of NEB, please refer to papers [8], [10], [11]

### B. CW complexes

A $k$ dimensional closed ball $\{x \in \mathcal{R}^k | \, ||x|| \leq 1\}$ is called a $k$-cell. A CW complex is a topological space $X$ defined by the follow inductive steps. The 0-skeleton $X^{(0)}$ of $X$ is a set of 0-cells. The 1-skeleton $X^{(1)}$ is created by gluing the endpoints of 1-cells to the 0-skeleton. Inductively, the $k$-skeleton $X^{(k)}$ are built by gluing the boundaries of $k$-cells to the $(k-1)$-skeleton $X^{(k-1)}$.

### C. Morse theory

Suppose $M$ be a compact manifold and a smooth Morse function $f : M \longrightarrow \mathcal{R}$ has non-degenerate critical points $t_1, ..., t_k \in M$ such that

$$p_0 < f(t_1) < p_1 < f(t_2) < \cdots < p_{k-1} < f(t_k) < p_k.$$

Suppose $M_p = f^{-1}((-\infty, p])$ is the sublevel set corresponding to $p \in \mathcal{R}$. It follows from Morse theory that $M_{p_i}$ is homotopy equivalent to a CW complex with a $\lambda_i$-cell for each critical point $t_i$.

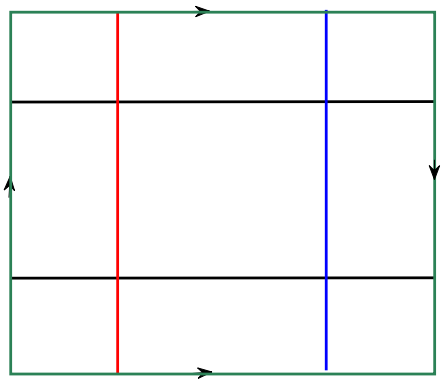

Fig.1. Denotation of Klein bottle as an identification space

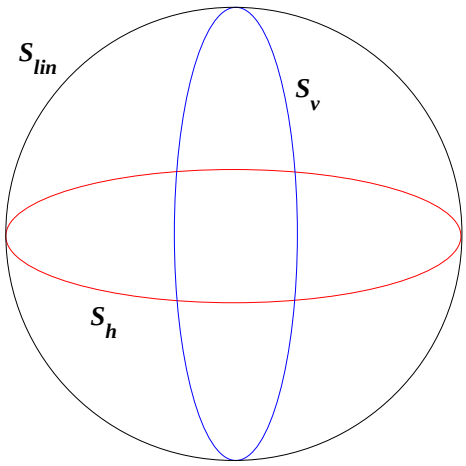


Fig.2. The three circle model.

### D. The three circles model

The Klein bottle can be represented by pasting a square as Fig.1. While pasting a square, three circles are created, one is the main circle ($S_{lin}$) informed by horizontal segments (black lines), the other two circles ($S_v$ and $S_h$) are informed from the vertical segments (red line and blue line) respectively, that is called the three circle model (Fig.2), represented by $C_3$. In the three circle space, the circles $S_v$ and $S_h$ intersect the main circle $S_{lin}$ in exactly two points, but they themselves do not intersect.

## III. The Data Sets of Natural Image Patches

We select data sets of $8\times 8$ and $9\times 9$ high-contrast patches from natural images of INRIA Holidays dataset [8]. Each data set consists of $5.5 \times 10^5$ high-contrast log patches. INRIA Holidays dataset is available at http://lear.inrialpes.fr/ jegou/data.php. Fig.3 is a sample.

Our spaces $X_8$ and $X_9$ are sets of $8\times 8$ and $9\times 9$ patches of high contrast created by the following steps.

Step 1. Select 550 images from INRIA Holidays dataset.

Step 2. Using MATLAB function rgb2gray to calculate the intensity at each pixel for each image.

Fig.3. A Sample from INRIA Holidays dataset

Step 3. We randomly choose 5000 $8\times 8$ and $9\times 9$ patches from each image.

Step 4. We consider each patch as a $n^2$-dimensional vector, and take the logarithm of each coordinate.

Step 5. For any vector $\mathbf{x}$=$(x_1, x_2, ..., x_n)$, we calculate the $D$-norm: $\| \mathbf{x} \|_D$. Two coordinates of $\mathbf{x}$ are neighbors, expressed by $i \sim j$, if the corresponding pixels in the $n \times n$ patch are adjacent. The formula of $D$-norm is: $\| \mathbf{x} \|_D = \sqrt{\sum_{i\sim j}(x_i - x_j)^2}$.

Step 6. We pick the patches that have a $D$-norm in the top $t = 20\%$ percent in each image.

Step 7. Subtract an average of all coordinates from each coordinate.

Step 8. We map $X_8$ ( $X_9$) into the unit sphere $S^{63}$ ($S^{80}$) by dividing each vector with its Euclidean norm.

Step 9. We randomly sample 50,000 points from $X_8$ and $X_9$ for computational convenience, the subspaces of $X_8$ and $X_9$ are represented by $\bar{X}_8$ and $\bar{X}_9$ respectively.

In this paper, we use set symbols similar as in the papers [7], [12], $\bar{X}_n(15000)$ is a random subset of $X_n$ with size 15000 $(n = 8, 9)$. We do not make the discrete cosine transform for these sets.

## IV. Computing Method

we give main steps of calculating method used in this section, for more details of the method, please refer to the paper [5].

Given a data set $X \subset \mathcal{R}^n$ from unknown probability density function $f : \mathcal{R}^n \longrightarrow [0, \infty)$. We take superlevel sets

$$X^\alpha = f^{-1}([\alpha, \infty)) = \{x \in \mathcal{R}^n | f(x) \geq \alpha\}$$

, the high dense regions of data set $X$ may give important topological information of $X$. We will construct CW complex models $Z^\alpha$ to approximate the superlevel sets $X^\alpha$.

We construct only the one-dimensional skeleton of the cell complex by following three steps. First step, we create a differentiable density estimator to approximate the unknown

probability density function. Second step, we acquire local maxima of the density estimate to give 0-cells. Third step, we randomly produce initial bands, then find the convergent bands by NEB, thus we obtain 1-cells.

### A. Density estimator

For a data set $X \subset \mathcal{R}^n$, let $\Phi_{x,\sigma} : \mathcal{R}^n \longrightarrow [0,\infty)$ be the probability density of a normal distribution centered at $x \in X$, we apply a differentiable density estimator $g(y) = |X|^{-1}\sum_{x\in X}\Phi_{x,\sigma}(y)$ to approach the unknown density.

### B. 0-cells

To find 0-cells, we randomly select an initial point $y_0 \in X$, and iteratively define a sequence $\{y_0, y_1, ...\}$ with $y_{n+1} = m(y_n)$, where $m(y) : \mathcal{R}^n \longrightarrow \mathcal{R}^n$ is the mean shift function given by the formula

$$m(y) = \frac{\sum_{x\in X}\Phi_{x,\sigma}(y)x}{\sum_{x\in X}\Phi_{x,\sigma}(y)}.$$

The sequence $\{y_n\}$ converges to a local maxima of $g$ [13]. In order to identify different 0-cells, we use single-linkage clustering to cluster the convergent points, and choose the densest member from each cluster as a 0-cell.

### C. 1-cells

For two 0-cells, there is a 1-cell between them if we find a convergent band between them by using NEB. For an initial band $[\mathbf{U}_0, \mathbf{U}_1, ..., \mathbf{U}_N]$, where $\mathbf{U}_0$ and $\mathbf{U}_N$ are 0-cells. Using a similar formula as (1), the total force on each midterm node $\mathbf{U}_i$ is computed by

$$\mathbf{F}_i = (||\mathbf{U}_{i+1} - \mathbf{U}_i|| - ||\mathbf{U}_i - \mathbf{U}_{i-1}||)\tau_i + c\bigtriangledown g(\mathbf{U}_i)|_\perp + \mathbf{F}_{sm}. \quad (2)$$

Where $c = (\sigma\sqrt{2\pi})^n\sqrt{e}$ is the gradient constant. Let $h_{\theta,\phi}(x) : [0,\pi] \longrightarrow [0,1]$ be a function defined by

$$h_{\theta,\phi}(x) = \begin{cases} 0, & x \le \theta \\ (1-\cos(\frac{x-\theta}{x-\phi}\pi))/2, & \theta < x < \phi \\ 1, & \phi \le x \end{cases}$$

Let $\alpha_i$ be the angle between $(\mathbf{U}_{i+1} - \mathbf{U}_i)$ and $(\mathbf{U}_i - \mathbf{U}_{i-1})$, the smoothing force $\mathbf{F}_{sm}$ is computed by $h_{\theta,\phi}(\alpha_i)(\mathbf{U}_{i+1} - 2\mathbf{U}_i + \mathbf{U}_{i-1})$, here $\theta = \pi/6$ and $\phi = \pi/2$.

## V. Experimental results

The author of the paper [7] used persistent homology to detect the topological structure of spaces $X_n$ of $n \times n$ natural image patches ($n = 8, 9$), and shown that the topologies of the core sets vary from a circle to a 3-circle model as decreasing of density estimator. Especially, there are core subsets $\bar{X}_n(300, 20)$ in $X_n$ ($n = 8, 9$) , whose homology is that of a circle. $X_8$ and $X_9$ have core subsets $\bar{X}_8(15, 20)$ and $\bar{X}_9(15, 20)$ respectively possessing the homology of the three circle model $C_3$. By using the method in [7], we can check that the core subsets $\bar{X}_8(20, 25)$ and $\bar{X}_9(20, 20)$ of $X_8$ and $X_9$ have the homology of the three circle model $C_3$ respectively.

Now we use NEB to analyse some subsets of $X_8$ and $X_9$, here we utilize two types subsets of $X_n$: (1) random subsets $\bar{X}_n(15000)$ of $X_n$ with size 15000; (2) core subsets $\bar{X}_n(k, p)$.

TABLE I. Data set information

| | $\bar{X}_8(15000)$ | $\bar{X}_8(300, 20)$ | $\bar{X}_8(15, 20)$ | $\bar{X}_8(20, 25)$ |
|---|---|---|---|---|
| size of data set | 15000 | 10000 | 10000 | 12500 |
| dimension $n$ | 64 | 64 | 64 | 64 |
| standard deviation $\sigma$ | 0.38 | 0.35 | 0.35 | 0.35 |

TABLE II. Data set information

| | $\bar{X}_9(15000)$ | $\bar{X}_9(300, 20)$ | $\bar{X}_9(15, 20)$ | $\bar{X}_9(20, 20)$ |
|---|---|---|---|---|
| size of data set | 15000 | 10000 | 10000 | 10000 |
| dimension $n$ | 81 | 81 | 81 | 81 |
| standard deviation $\sigma$ | 0.30 | 0.38 | 0.35 | 0.38 |

### A. $8 \times 8$ patches

The data sets used for $X_8$ are shown in Table 1. For the set $\bar{X}_8(15000)$, we let standard deviation $\sigma = 0.38$, we get four 0-cells with densities 0.7664, 0.7826, 0.877, and 0.8818 respectively, and four 1-cells having densities 0.7597, 0.7664, 0.7672 , and 0.7772 respectively, these cells produce a loop. Therefore for $\alpha = 0.7597$, the $Z^\alpha$ is a circle (Fig.4). When we choose standard deviation $\sigma = 0.30$, we have four 0-cells having densities in [$1.02\times10^6$, $1.356\times10^6$] and four 1-cells with densities in [$8.001\times10^5$, $8.566\times10^5$], these cells also produce a circle.

For $\bar{X}_8(300, 20)$, we take the value of standard deviation $\sigma = 0.35$, we get four 0-cells having densities of 277.2, 294.5, 396.5 and 401.7 and four 1-cells having densities of 216.1, 224.1, 227.5 and 228.9, all these cells compose a circle (Fig.5).

For $\bar{X}_8(15, 20)$, let $\sigma = 0.35$, we find four 0-cells and four 1-cells which compose a circle (Fig.6). The four 0-cells have densities of 263.6, 279.4, 366, and 378.9, the four 1-cells have densities of 207.1, 217.3, 218.7, and 218.9. When we take $\sigma$=0.30, and 0.38, we obtain similar results as for $\sigma = 0.35$. For example, for $\sigma = 0.38$, the four 0-cells have densities in [1.649, 2.332] and the four 1-cells have densities in [1.42, 1.497].

For $\bar{X}_8(20, 25)$, we have the similar result as $\bar{X}_8(15, 20)$. Taking $\sigma = 0.25$, 0.30, 0.35 and 0.38, we get four 0-cells and four 1-cells for each case which form a circle. For example, when $\sigma = 0.35$, the four 0-cells have densities 240.7, 253.2, 330.1, 335.8 and the four 1-cells have densities 198.4, 205.5, 205.7, 206.1 respectively, these cells form a circle (Fig.7).

As shown in [7], the subspace $\bar{X}_8(15, 20)$ ($\bar{X}_8(20, 25)$) of $X_8$ has same homology as the three circle model $C_3$, but we can not detect that $\bar{X}_8(15, 20)$ ($\bar{X}_8(20, 25)$) has the topology of $C_3$ by using the current method.

### B. $9 \times 9$ patches

In this section we utilize the computing method for two kind of data sets in Table 2. We consider the set $\bar{X}_9(15000)$ for standard deviation $\sigma = 0.30$, we find four 0-cells, whose densities are $1.138\times10^8$, $1.15\times10^8$, $1.587\times10^8$, $1.627\times10^8$ respectively, and four 1-cells with densities of $9.364\times10^7$, $9.405\times10^7$, $9.408\times10^7$, $9.884\times10^7$, all these cells form a circle. Thus $\alpha = 9.364 \times 10^7$, the $Z^\alpha$ is a circle (Fig.8). If we take $\sigma = 0.35$, we get four 0-cells with densities in [864, 1091], and four 1-cells having densities in [822.7, 850.3], which also compose a circle.

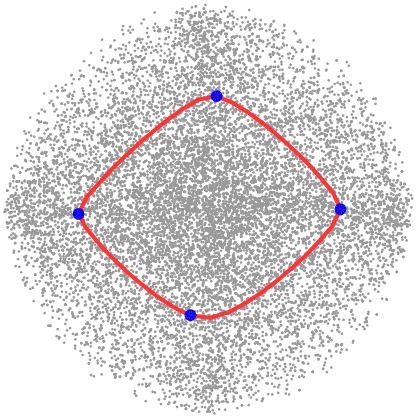

Fig.4. $\bar{X}_8(15000)$ and the circle $Z^{0.7597}$, projected to a plane.

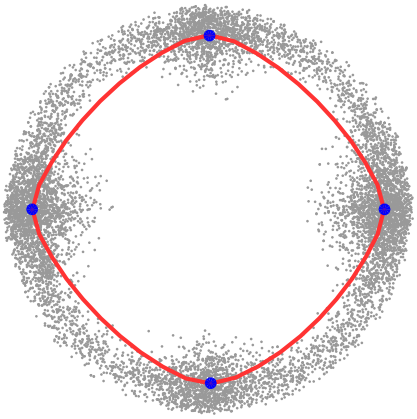

Fig.5. $\bar{X}_8(300, 20)$ and the circle $Z^{216.1}$, projected to a plane.

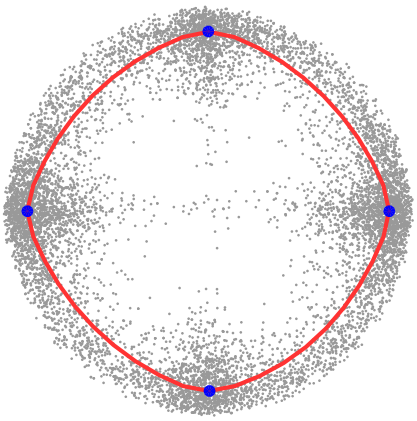

Fig.6. $\bar{X}_8(15, 20)$ and the circle $Z^{207.1}$, projected to a plane.

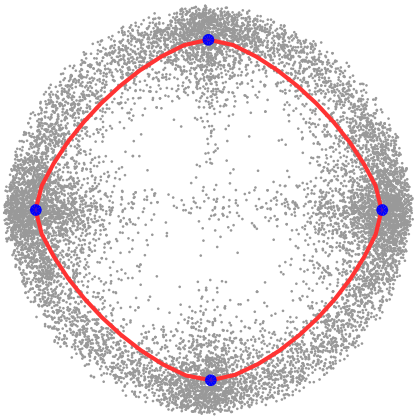

Fig.7. $\bar{X}_8(20, 25)$ and the circle $Z^{198.4}$, projected to a plane.

For $\bar{X}_9(300, 20)$, when we take $\sigma = 0.35$, we have four 0-cells with densities in [23800, 35840] and four 1-cells having densities in [1910, 2031], all these cells form a circle (Fig.9). If we let $\sigma$=0.25, 0.30, and 0.38, we get similar results as for $\sigma = 0.35$. However the densities of cells decrease as increasing of standard deviation, for example, when $\sigma = 0.38$, we get four 0-cells having densities in [3.704, 5.504] and four 1-cells with densities in [3.263, 3.436].

We take standard deviation $\sigma$=0.20, 0.25, 0.30, 0.35, and 0.38 for $\bar{X}_9(15, 20)$, for each case we obtain four 0-cells and four 1-cells, these cells compose a circle. For example, if $\sigma = 0.35$, four 0-cells have densities 2254, 2308, 3240, and 3333, four 1-cells have densities 1817, 1863, 1908, and 1935 respectively, these cells form a circle (Fig.10).

For $\bar{X}_9(20, 20)$, we get the similar result as $\bar{X}_9(15, 20)$. For example, when $\sigma = 0.38$, we find four 0-cells with densities in [3.548, 5.138] and four 1-cells with densities in [3.143, 3.292], these cells form a circle (Fig.11).

We take various values of standard deviation $\sigma$ and do experiments for them, but we can not find that $\bar{X}_9(15, 20)$ ($\bar{X}_9(20, 20)$) has the homology of $C_3$ by the current method.

## VI. Conclusions

In this paper we utilize the nudged elastic band technique to analyse spaces of $8\times8$ and $9\times9$ natural image patches, and we get some similar results as the papers [2], [7], which show that the results got in this paper and [2], [7] are native properties of natural image patches, they do not rest on the methods and databases. We experimentally show that the spaces of high-contrast $8\times8$ and $9\times9$ patches have different subsets modeled as a circle. By matching the results (method) of this paper with the results (method) of the papers [2], [7], we discover that the most advantage of the method is its simplicity. For example, to model $\bar{X}^8(300, 20)$ as a circle using cell complexes, we only use four 1-cells, if we model $\bar{X}^8(300, 20)$ as a circle using witness complexes, we may need several tens of thousands witness complexes. The disadvantages of the method are that to create higher dimensional cells is more difficult [5] and it may only detect coarse topology of a data-set.

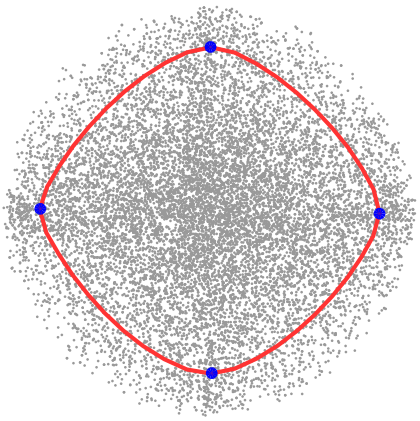

Fig.8. $\bar{X}_9(15000)$ and the circle $Z^{9.364\times10^7}$, projected to a plane.

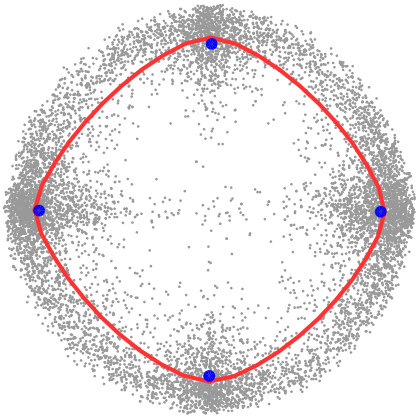

Fig.9. $\bar{X}_9(300,20)$ and the circle $Z^{1910}$, projected to a plane.

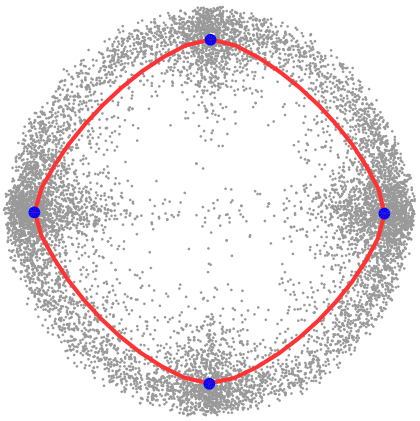

Fig.10. $\bar{X}_9(15,20)$ and the circle $Z^{1817}$, projected to a plane.

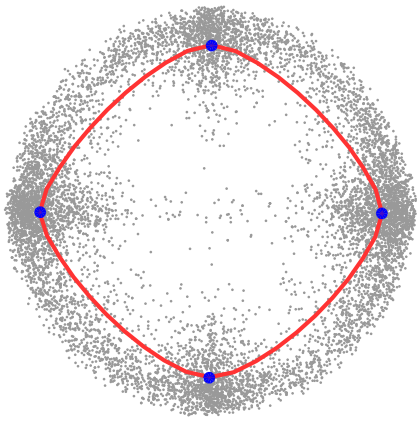

Fig.11. $\bar{X}_9(20,20)$ and the circle $Z^{3.143}$, projected to a plane.

## ACKNOWLEDGEMENTS

The authors are very grateful to the reviewers for valuable comments.

Project supported by the National Natural Science Foundation of China (Grant No.61471409).

## REFERENCES

[1] H. Adams and G. Carlsson, *On the nonlinear statistics of range image patches*, SIAM J. Imag. Sci., **2** (2009), 110–117.

[2] G. Carlsson, T. Ishkhanov, V. de Silva, A. Zomorodian, *On the local behavior of spaces of natural images*, Internat. J. Computer Vision, 76 (2008), pp. 1–12.

[3] G. Carlsson, *Topology and data*, Bulletin (New Series) of the American Mathematical Society, 46 (2009), pp. 255–308.

[4] A. Zomorodian, *Topological data analysis, Advances in Applied and Computational Topology* (Proceedings of Symposia in Applied Mathematics), A. Zomorodian, eds., American Mathematical Society, 70 (2012), pp. 1–39.

[5] H. Adams, A. Atanasov, and G. Carlsson, *Nudged elastic band in toplogical data analysis*, Topological Methods in Nonlinear Analysis, 45 (2015), pp. 247–272.

[6] A. B. Lee, K. S. Pedersen, and D. Mumford, *The non-linear statistics of high-contrast patches in natural images*, Internat. J. Computer Vision, 54 (2003), pp. 83–103.

[7] S. Xia, *An Analysis on Natural Image* $8\times8$ *and* $9\times9$*-Patches*, submitted.

[8] H. Jegou, M. Douze, and C. Schmid, *Hamming Embedding and Weak geometry consistency for large scale image search*, Proceedings of the 10th European conference on Computer vision, October (2008), pp. 304–317.

[9] D. Sheppard, R. Terrell, and G. Henkelman, *Optimization methods for finding minimum energy paths*, Journal Chemical Physics, 128 (2008), pp. 134106-1–10.

[10] G. Henkelmana and H. Jónsson, *Improved tangent estimate in the nudged elastic band method for finding minimum energy paths and saddle points*, Journal Chemical Physics, 113 (2000), pp. 9978–9985.

[11] G. Henkelman, B. Uberuaga, H. Jónsson, *A climbing image nudged elastic band method for finding saddle points and minimum energy paths*, Journal Chemical Physics, 112 (2000), pp. 9901–9904.

[12] S. Xia, *A topological analysis of high-contrast patches in natural images*, J. Nonlinear Sci. Appl., 9 (2016), pp. 126–138.

[13] Y. Cheng, *Mean shift, mode seeking, and clustering*, IEEE Trans. Pattern Anal., 17 (1995), pp. 790–799.